Cognitive Computation (2019) 11:644–655
https://doi.org/10.1007/s12559-019-09658-8

Improving the Recall Performance of a Brain Mimetic Microcircuit Model

Vassilis Cutsuridis[1]

Received: 8 February 2019 / Accepted: 30 May 2019 / Published online: 13 June 2019

Abstract

The recall performance of a well-established canonical microcircuit model of the hippocampus, a region of the mammalian brain that acts as a short-term memory, was systematically evaluated. All model cells were simplified compartmental models with complex ion channel dynamics. In addition to excitatory cells (pyramidal cells), four types of inhibitory cells were present: axo-axonic (axonic inhibition), basket (somatic inhibition), bistratified cells (proximal dendritic inhibition) and oriens lacunosum-moleculare (distal dendritic inhibition) cells. All cells' firing was timed to an external theta rhythm paced into the model by external reciprocally oscillating inhibitory inputs originating from the medial septum. Excitatory input to the model originated from the region CA3 of the hippocampus and provided context and timing information for retrieval of previously stored memory patterns. Model mean recall quality was tested as the number of stored memory patterns was increased against selectively modulated feedforward and feedback excitatory and inhibitory pathways. From all modulated pathways, simulations showed recall performance was best when feedforward inhibition from bistratified cells to pyramidal cell dendrites is dynamically increased as stored memory patterns is increased with or without increased pyramidal cell feedback excitation to bistratified cells. The study furthers our understanding of how memories are retrieved by a brain microcircuit. The findings provide fundamental insights into the inner workings of learning and memory in the brain, which may lead to potential strategies for treatments in memory-related disorders.

Keywords Hippocampus · Inhibition · Excitation · Bistratified cell · Schaffer collateral · Medial septum

Introduction

We are continually bombarded with sensory information, some of which we remember and some of which sparks the recall of old memories. Some aspects of how the brain may store and recall information were captured in mathematical artificial neural network models known as associative memories, which were first developed over 50 years ago [35, 37]. These models worked by storing patterns of information via changes in the strengths of connections between simple computing units that mimicked the operation of neurons in the brain in a very simple way. Old memories were recalled when a noisy or partial version of a previously stored patterns was presented to the network. However, these devices were not very flexible. They had to be told when to store a pattern and when they were supposed to recall a memory. The types of information they could store were quite limited.

In 2010, a much more flexible model was introduced that controlled for itself the storage and recall of patterns of information arriving at unpredictable rates [10]. The model was based upon the many details we knew of the neuronal hippocampal circuit, a part of the mammalian brain that acts as a short-term memory. The model explored the functional roles of somatic, axonic and dendritic inhibition in the encoding and retrieval of memories in region CA1 of the hippocampus. It showed how theta modulated inhibition separated encoding and retrieval of memories in the hippocampus into two functionally independent processes. It predicted that somatic inhibition allowed generation of dendritic calcium spikes that promoted synaptic long-term plasticity (LTP), while minimizing cell output. Proximal dendritic inhibition controlled both cell output and suppressed dendritic calcium spikes, thus preventing LTP, whereas distal dendritic inhibition removed

Electronic supplementary material The online version of this article (https://doi.org/10.1007/s12559-019-09658-8) contains supplementary material, which is available to authorized users.

✉ Vassilis Cutsuridis
vcutsuridis@lincoln.ac.uk; vcutsuridis@gmail.com

[1] School of Computer Science, Brayford Pool, University of Lincoln, Lincoln LN6 7TS, UK

interference from spurious memories during recall. The mean recall quality of the model was tested as function of memory patterns stored (see Fig. 14 in [10]). Recall dropped with a larger number of patterns stored due to interference from previously stored memories. Proximal dendritic inhibition was held constant as the number of memory patterns stored was increased.

In this article, the Cutsuridis et al. [10] model is extended to uncover the biophysical factors that will improve its memory capacity and recall performance. In contrast to previous models [7–10] where the strength of the bistratified cell (BSC) inhibition to pyramidal cell (PC) dendrites was held constant, the present model examined how selective modulation of feedforward and feedback excitatory and inhibitory pathways targeting BSC and/or PCs may influence the BSC thresholding capacity to remove spurious activity and improve the mean recall quality of PCs as a larger number of memories is stored.

Materials and Methods

Figure 1 in the main text illustrates the simulated microcircuit model of the CA1 network. The model consists of 100 PCs, one axo-axonic cell (AAC), two basket cells (BCs), 1 BSC and one oriens lacunosum-moleculare (OLM) cell. All simulations were performed using NEURON [17] running on a PC with four CPUs under Windows 8.

Simplified morphologies including the soma, apical and basal dendrites and a portion of the axon were used for each cell type. The biophysical properties of each cell were adapted from cell types reported in the literature, which were extensively validated against experimental data in [27–30]. The complete mathematical formalism of the model has been described elsewhere [10]. Schematic representations of the model cells are depicted in Supplementary Figures 1–2. The dimensions of the somatic, axonic and dendritic compartments of the model cells are presented in Supplementary Table 1. The parameters of all passive and active ionic conductances used in the model are listed in Supplementary Tables 2–4. The synaptic waveform parameters are given in Supplementary Table 5, and synaptic conductances are listed in Supplementary Table 6. Experimental support of the choices of the various parameters is found in supplementary online material (SOM).

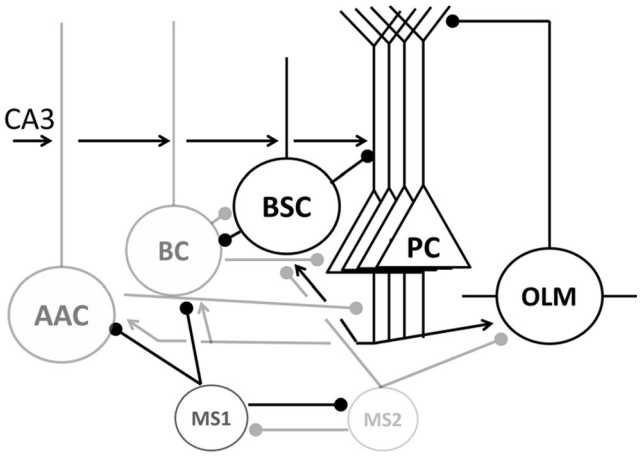

Fig. 1 Hippocampal CA1 microcircuit showing major cell types and their connectivity. PC pyramidal cell, AAC axo-axonic cell, BC basket cell, BSC bistratified cell, EC entorhinal cortex input, CA3 CA3 Schaffer collateral input, MS1 medial septum cell population 1 (firing at theta trough), MS2 medial septum cell population 2 (firing at theta peak). Black arrows: active excitatory input; light gray arrows: inactive excitatory input; black filled circles: active inhibitory input; light gray filled circles: inactive inhibitory input

Pyramidal Cells

Each PC had 15 compartments (see Supplementary Figure S1), each containing a calcium pump and buffering mechanism, calcium-activated slow AHP and medium AHP K^+ currents, an HVA L-type Ca^{2+} current, an HVA R-type Ca^{2+} current, an LVA T-type Ca^{2+} current, an h current, a fast sodium and a delayed rectifier K^+ current, a slowly inactivating M-type K^+ current and a fast inactivating A-type K^+ current [27, 28].

Each PC's soma rested in the stratum pyramidale (SP), while its dendrites extended across the strata from stratum oriens (SO) to stratum radiatum (SR) and stratum lacunosum-moleculare (SLM). Each PC received somatic synaptic inhibition from the BCs, mid-dendritic excitation from Schaffer collaterals (CA3-PCs), proximal excitation from around 1% of other CA1 PCs in the network (recurrent collaterals) [1, 3], axonic inhibition from the AACs, spatially-distributed (six contacts) proximal dendritic synaptic inhibition from BSCs and distal synaptic inhibition on each SLM dendritic branch from the OLM cell.

Axo-Axonic Cell

Each AAC had 17 compartments (see Supplementary Figure S2), which included a leak conductance, a sodium current, a fast delayed rectifier K^+ current, an A-type K^+ current, L- and N-type Ca^{2+} currents, a Ca^{2+}-dependent K^+ current and a Ca^{2+}- and voltage-dependent K^+ current [29]. Each AAC soma rested primarily in the SP, while its dendrites extended across the strata from SO to SR and SLM. AACs received excitatory inputs from the CA3 Schaffer collateral to their SR dendrites. In addition, the axo-axonic cells received inputs from active CA1 pyramidal cells in their SR medium and thick dendritic compartments as well as inhibitory input from the septum in their SO thick dendritic compartments [3, 13].

Basket Cell

Each BC had 17 compartments (see Supplementary Figure S2), containing a leak conductance, a sodium current, a fast delayed rectifier K^+ current, an A-type K^+ current, L- and N-type Ca^{2+} currents, a Ca^{2+}-dependent K^+ current and a Ca^{2+}- and voltage-dependent K^+ current [29]. All BCs' somas rested in SP, whereas their dendrites extended from SO to SLM. All BCs received excitatory connections from the CA3 Schaffer collaterals to their medium SR dendrites and from active pyramidal cells to their medium and thick SR dendritic compartments and inhibitory connections from neighbouring BCs and BSCs in their soma [12] and from the medial septum in their SO thick dendritic compartments.

Bistratified Cell

Each BSC had 13 compartments (see Supplementary Figure S2), which included the same ionic currents as the BCs and AACs. All BSCs' somas rested in the SR, whereas their dendrites extended from SO to SR. All BSCs received excitatory connections from the CA3 Schaffer collaterals in their medium SR dendritic compartments and from the active CA1 PCs in their thick SO dendrites and inhibitory connections from the medial septum in their thick SO dendritic compartments and from neighbouring BCs and BSCs in their somas.

OLM Cell

Each OLM cell had four compartments (see Supplementary Figure S2), which included a sodium (Na^+) current, a delayed rectifier K^+ current, an A-type K^+ current and an h current [30]. Each OLM cell's soma and basal dendrites rested in SP, whereas its axon extended from SP to SLM. Each OLM cell received excitatory connections from the active PCs in their basal dendrites as well as inhibitory connections from the medial septum in their soma.

Model Inputs

The model was driven by a CA3 Schaffer collateral excitatory input and an MS inhibitory input. The CA3 input was modelled as the firing of 20 out of 100 CA3 pyramidal cells at an average gamma frequency of 40 Hz (spike trains only modelled and not the explicit cells) (see Figs. 2 and 3). PCs, BCs, AACs and BSCs received CA3 input in their medial SR dendrites. On the other hand, the MS input was modelled with the rhythmic firing of two populations of 10 septal cells each modulated at opposite phases of a theta cycle (180° out of phase) [4]. Septal cell output was modelled as bursts of action potentials using a presynaptic spike generator. Each spike train consisted of bursts of action potentials at a mean frequency of 8 Hz for a half-theta cycle (70 ms) followed by a half-theta cycle of silence. Due to 8% noise in the inter-spike intervals, the 10 spike trains in each septal population were asynchronous. MS2 input provided GABA-A inhibition to BSCs and OLMs during the storage cycle (not simulated here; see Fig. 3), whereas MS1 input provided GABA-A inhibition to AACs and BCs during the retrieval cycle (see Fig. 3).

Synaptic Properties

In the model, AMPA, NMDA, GABA-A and GABA-B synapses were considered. GABA-A were present in all strata, whereas GABA-B were present in medium and distal SR and SLM dendrites. AMPA synapses were present in strata LM (EC connections) and radiatum (CA3 connections), whereas NMDA were present only in stratum radiatum (CA3 connections).

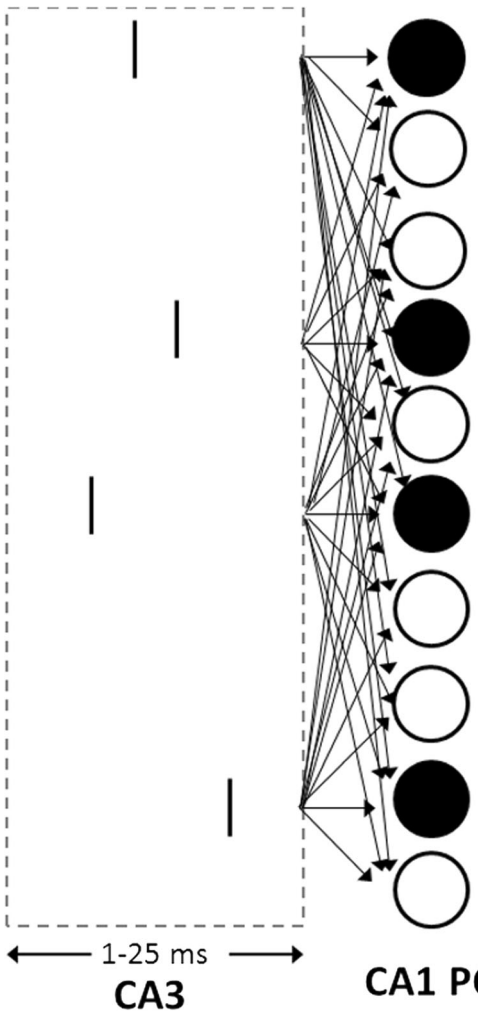

Fig. 2 Model CA3 inputs to CA1 microcircuit. CA3 input arrives asynchronously in CA1 PC dendrites between 1 and 25 ms. All PCs receive non-selectively the CA3 input

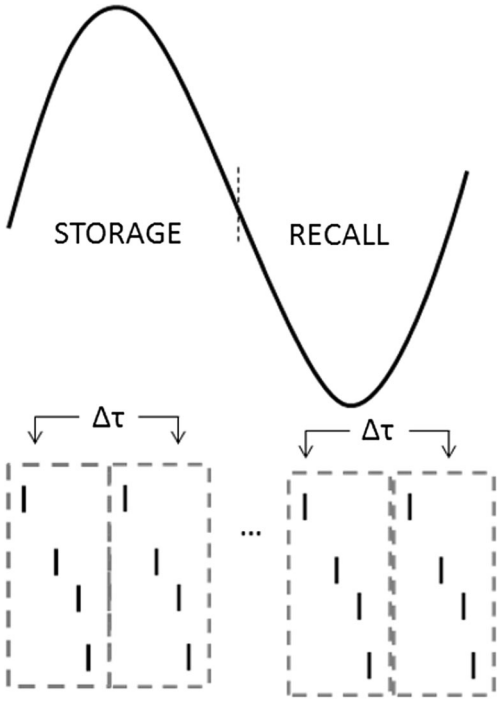

Fig. 3 Graphical representation of input presentation in the model. Inputs are presented continuously at gamma frequency, throughout the storage and recall cycles of the theta rhythm. Each input window (gray rectangular window) is repeated every $\Delta\tau = 25$ ms

Network Testing

To test the recall performance of the model, the methodology described in Cutsuridis et al. [10] study was replicated. More specifically, a memory pattern was stored by generating weight matrices based on a clipped Hebbian learning rule; these weight matrices were used to pre-specify the CA3 to CA1 PC connection weights. Without loss of generality, the input (CA3) and output (CA1) patterns were assumed to be the same, with each pattern consisting of 20 randomly chosen PCs out of the population of 100. The 100×100 dimensional weight matrix was created by setting matrix entry (i, j), $w_{ij} = 1$ if input PC i and output PC j are both active in the same pattern pair; otherwise, weights are 0. Any number of pattern pairs could be stored to create this binary weight matrix. The matrix was applied to our network model by connecting a CA3 input to a CA1 PC with a high AMPA conductance (gAMPA = 1.5 nS) if their connection weight was 1 or with a low conductance (gAMPA = 0.5 nS) if their connection was 0. This approach is in line with experimental evidence that such synapses are 2-state in nature [26].

Recall Performance

The recall performance metric used for measuring the distance between the recalled output pattern, A, from the required output pattern, A^*, was the correlation (i.e., degree of overlap) metric, calculated as the normalized dot product:

$$C = \frac{A \cdot A^*}{\left(\sum_{i=1}^{NA} A_i \cdot \sum_{j=1}^{NA} A_j^*\right)} \quad (1)$$

where N is the number of output units. The correlation takes a value between 0 (no correlation) and 1 (the vectors are identical). The higher the correlation is, the better the recall performance.

Model Selection

As in the Cutsuridis et al. [10] model, the BSC inhibition to PC dendrites is hypothesized to mediate thresholding of PC firing during recall. In the *canonical model* (see Fig. 5a), BSC inhibition to PC dendrites is held constant as the number of stored patterns increases. The recall quality of the canonical model decreases as more and more memories are loaded into the network (see Fig. 14 in Cutsuridis et al.'s [10] study and in Fig. 5b herein). To test the influence of feedforward and feedback excitation and inhibition to the BSC thresholding operation to remove unwanted spurious activity and subsequently improve the model's recall performance as the number of stored patterns increased, the synaptic strength of selective excitatory and inhibitory pathways to BSC and PC soma and dendrites was dynamically modulated as the number of stored patterns increased:

1. Increased CA3 feedforward excitation to BSC SR dendrites (*model 1*).
2. Increased BSC feedforward inhibition to PC dendrites (*model 2*).
3. Increased PC feedback excitation to BSC SO dendrites (*model 3*).
4. Increased CA3 feedforward excitation to BSC SR dendrites and BSC feedforward inhibition to PC dendrites (*model 4*).
5. Increased BSC feedforward inhibition to PC dendrites and PC feedback excitation to BSC SO dendrites (*model 5*).
6. Increased CA3 feedforward excitation to BSC SR dendrites and PC feedback excitation to BSC SO dendrites (*model 6*).

Comparative analysis of all above six models' recall performance against the canonical model is depicted in Fig. 12. Synaptic conductance parameters from all six models including the canonical one are found in Table 1.

Results

A set of patterns were stored without recourse to a learning rule by generating a weight matrix based on a clipped

Table 1 Synaptic conductance parameters (in microSiemens) for all seven models. Text in parenthesis signifies the number of patterns stored in the network

Canonical model				
		Postsynaptic		
		BSC	PC (GABA-A)	PC (GABA-B)
Presynaptic	CA3	0.00015 (P1-P40)		
	BSC		0.006 (P1-P40)	0.0008 (P1-P40)
	PC	0.0005 (P1-P40)		
Model 1				
		Postsynaptic		
		BSC	PC (GABA-A)	PC (GABA-B)
Presynaptic	CA3	0.00015 (P1) 0.00015 x 2 (P2) 0.00015 x 3.2 (P5) 0.00015 x 3.3 (P10) 0.00015 x 3.6 (P20) 0.00015 x 3.8 (P40)		
	BSC		0.006 (P1-P40)	0.0008 (P1-P40)
	PC	0.0005 (P1-P40)		
Model 2				
		Postsynaptic		
		BSC	PC (GABA-A)	PC (GABA-B)
Presynaptic	CA3	0.00015 (P1-P40)		
	BSC		0.006 (P1) 0.009 (P2-P40)	0.0008 (P1) 0.0015 (P2) 0.0025 (P5) 0.0045 (P10-P40)
	PC	0.0005 (P1-P40)		
Model 3				
		Postsynaptic		
		BSC	PC (GABA-A)	PC (GABA-B)
Presynaptic	CA3	0.00015 (P1-P40)		
	BSC		0.006 (P1-P40)	0.0008 (P1-P40)
	PC	0.0005 (P1) 0.001 (P2) 0.007 (P5) 0.045 (P10-P40)		
Model 4				
		Postsynaptic		
		BSC	PC (GABA-A)	PC (GABA-B)
Presynaptic	CA3	0.00015 (P1) 0.00015 x 1.4 (P2) 0.00015 x 1.5 (P5-P10) 0.00015 x 1.7 (P20-P40)		
	BSC		0.006 (P1-P40)	0.0008 (P1) 0.0012 (P2) 0.002 (P5-P10) 0.0026 (P20-P40)
	PC	0.0005 (P1-P40)		
Model 5				
		Postsynaptic		
		BSC	PC (GABA-A)	PC (GABA-B)
Presynaptic	CA3	0.00015 (P1-P40)		
	BSC		0.006 (P1) 0.009 (P2-P40)	0.0008 (P1) 0.001 (P2) 0.0025 (P5)

Table 1 (continued)

				0.0045 (P10-P40)
	PC	0.0005 (P1) 0.0008 (P2) 0.0013 (P5) 0.0045 (P10-P40)		
Model 6				
		Postsynaptic		
		BSC	PC (GABA-A)	PC (GABA-B)
Presynaptic	CA3	0.00015 (P1) 0.00015 x 1.5 (P2) 0.00015 x 3.5 (P5-P20) 0.00015 x 4.5 (P40)		
	BSC		0.006 (P1-P40)	0.0008 (P1-P40)
	PC	0.0005 (P1) 0.001 (P2) 0.006 (P5-P40)		

Hebbian learning rule and using the weight matrix to prespecify the CA3 to CA1 PC connection weights. To test recall of a previously stored memory pattern in the canonical model, the associated input pattern was applied as a cue in the form of spiking of active CA3 inputs (those belonging to the pattern) distributed within a gamma frequency time window. The entire cue pattern was repeated at gamma frequency (40 Hz). During the retrieval, only the BSCs and OLM cells were switched on, whereas the AACs and BCs were switched off. The CA3 spiking drove the CA1 PCs plus the BSCs. The EC input (not depicted here), which excite the distal dendrites of PCs, AACs and BCs, is disconnected during the retrieval.

The recall of a memory pattern is shown in Fig. 4. Figure 4a and b are raster plots of the spiking of (a) septal (top 20 rows) and CA3 (bottom 100 rows) input and (b) CA1 PCs, respectively. The CA1 PCs are active two or three times during recall, with their spiking activity being a very close match to the stored pattern. Three recall cycles are shown, following an initialization period of 50 ms.

Recall performance is calculated by measuring the CA1 PC spiking activity during a sliding 10 ms time window (Fig. 4c shows the spike counts in each time window). For each time, window a binary vector of length 100 is formed, with entries having a value of 1 if the corresponding PC spikes in the window. The correlation (normalized dot product; Eq. (1)) of this vector with the expected pattern vector is calculated to give a measure of recall quality between 0 and 1, with 1 corresponding to perfect recall. Figure 4d shows recall quality over time. When CA1 PC spiking occurs, always the first PCs to fire are the ones belonging to the stored pattern, and quality goes to one. All recall events in this example are perfect, and the recall quality averages at 1 (Fig. 4d).

Below I discuss the hypothesis of each of the previously identified models (see "Model Selection") including that of the canonical model (BSC inhibition to PC dendrites is constant) and demonstrate their recall performances as the number of stored patterns increases. Comparative analysis of all models' recall performance is depicted in Fig. 12. Synaptic conductance parameters from all seven models are found in Table 1.

Canonical Model

The canonical model is depicted in Fig. 5a. The BSC inhibitory synaptic strength to PC dendrites is held constant as the number of stored patterns is increased. As the number of patterns stored is increased, the average recall quality is degraded, because PCs receive more excitation from cue patterns they did not belong to, leading to spurious firing (see Fig. 5b).

Model 1—Increased CA3 Feedforward Excitation to BSC SR Dendrites

Model 1 is depicted in Fig. 6a. The hypothesis with this model is that as the CA3 Schaffer collateral feedforward excitation to BSC SR dendrites is increased, the BSC firing rate will also increase and hence the efficacy of the BSC inhibition to proximal PC dendrites. Increased BSC efficacy (i.e., inhibitory threshold) will lead to less spurious PC firing as the number of patterns stored is increased. As it is evident from Fig. 6b, the recall performance of this model is excellent for up to 10 stored patterns, slightly decreases to 0.91 for 20 stored patterns but falls to 0.54 when 40 memory patterns are stored. The possible minimum quality when all PCs become active is 0.44.

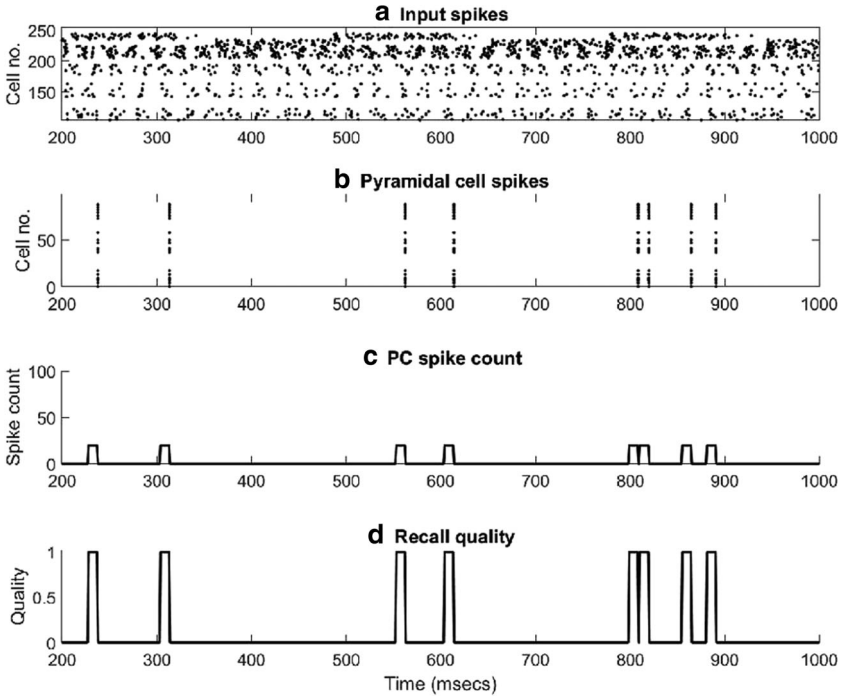

Fig. 4 Example of pattern recall. **a** Raster plot showing the septal (top 20) and CA3 input (bottom 100) spikes. **b** Raster plot showing CA1 PC activity—the only active cells are those belonging to the stored pattern. **c** PC spike count in a sliding 10-ms bin. **d** Recall quality in a sliding 10 ms bin

Model 2—Increased BSC Feedforward Inhibition to PC Dendrites

Model 2 is depicted in Fig. 7a. The assumption here is that increasing the BSC inhibition to PC dendrites, then PC spurious firing will decrease. Both GABA-A and GABA-B conductances were increased with the GABA-B having the strongest effect on removing the spurious activities as the stored patterns increased. The recall performance was perfect ($C = 1$) for the first 20 patterns stored (see Fig. 7b). When 40 patterns were stored, the mean recall quality dropped to 0.79.

Model 3—Increased PC Feedback Excitation to BSC SO Dendrites

Model 3 is depicted in Fig. 8a. The hypothesis with this model is that the effect of increased PC feedback excitation to BSC SO dendrites would cause BSC to fire more, and thus, the BSC inhibitory threshold mechanism efficiency of removing spurious PC activities will increase. Compared to previous models, the mean recall quality of this model decreased even for the first five stored patterns ($C = 0.83$) (see Fig. 8b). For 40 stored patterns, the mean recall quality was 0.6.

Model 4—Increased CA3 Feedforward Excitation to BSC SR Dendrites and BSC Feedforward Inhibition to PC Dendrites

Model 4 is depicted in Fig. 9a. The hypothesis with this model was that when increases in the CA3 feedforward excitation to BSC dendrites causing the BSC firing rate to increase and increases in BSC feedforward GABA-A and GABA-B inhibitory efficacy to proximal PC dendrites would undoubtedly raise the BSC thresholding efficiency to remove spurious

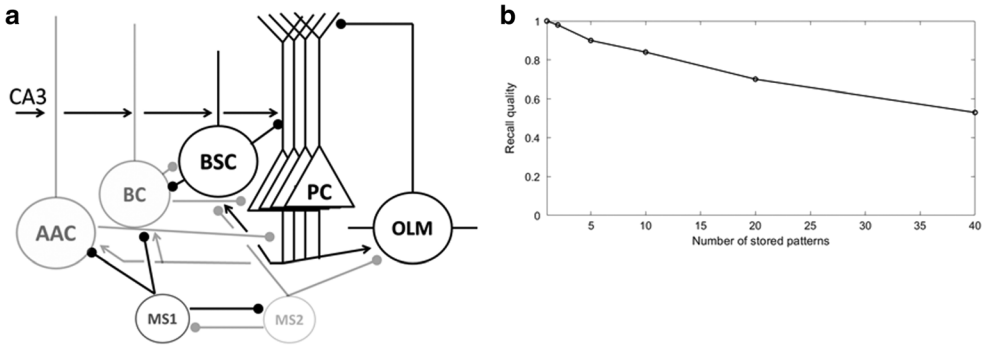

Fig. 5 **a** Canonical CA1 circuit model. The strength of BSC inhibition onto the PC dendrites is held constant as the number of stored patterns is increased. **b** Recall quality of the canonical CA1 circuit model as a function of number of patterns stored. Recall drops with a larger number of patterns due to an increase in spurious PC activity. Note that the possible minimum quality when all cells become active is 0.44

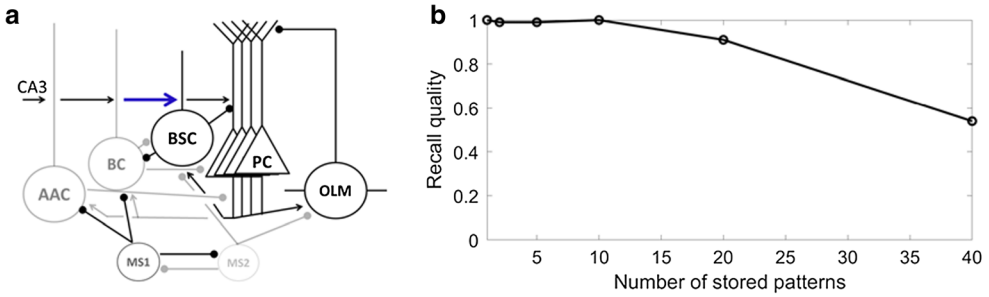

Fig. 6 **a** CA1 circuit model 1. Increased CA3 feedforward excitation to BSC SR dendrites (depicted as blue solid line) as the number of stored patterns is increased. **b** Recall quality of the model as a function of number of patterns stored. Quality is perfect ($C = 1$) for up to 10 stored patterns, slightly decreases to 0.91 for 20 stored patterns but falls to 0.54 when 40 memory patterns are stored. Note that the possible minimum quality when all cells become active is 0.44

activity and improve recall quality. Indeed, the mean recall quality was perfect ($C = 1$) for the first 10 patterns stored, dropped slightly ($C = 0.9$) for 20 stored patterns and became 0.64 for 40 stored patterns (see Fig. 9b).

Model 5—Increased BSC Feedforward Inhibition to PC Dendrites and PC Feedback Excitation to BSC SO Dendrites

Model 5 is depicted in Fig. 10a. This model's hypothesis was the same as in model 4. However, the mean recall quality of this model when 40 patterns were stored was 0.8 (see Fig. 10b). Its performance for the first 20 stored patterns (see Fig. 10b) was comparable to model 4.

Model 6—Increased CA3 Feedforward Excitation to BSC SR Dendrites and PC Feedback Excitation to BSC SO Dendrites

Model 6 is depicted in Fig. 11a. The hypothesis here was if both feedback and feedforward excitation to BSC will increase its firing rate, then perhaps these factors alone would sufficient to improve the BSC threshold mechanism to remove spurious activity. The mean recall quality of this model for the first 10 patterns was perfect ($C = 1$) but decreased to 0.86 and 0.55 for 20 and 40 patterns (see Fig. 11b), respectively.

Discussion

What Have We Learned from the Model

A biologically realistic CA1 network model with morphologically simplified neurons has been extended to investigate the biophysical factors that improved its recall performance as more and more memory patterns were stored in the synapses of its principal (pyramidal) cells. The model demonstrated the feasibility of the separation of storage and recall processes into separate theta subcycles due to theta modulated intra- and extra-hippocampal inhibition. The model simulated the timing of different extra- and intra-hippocampal cells types relative to the theta rhythm in anesthetized animals [4, 19, 20] and proposed functional roles for different classes of intra-hippocampal inhibitory interneurons in the retrieval (and encoding) of information.

The analyses presented here conclusively showed that *only* increases in the inhibitory synaptic efficacy (*weight*) of BSCs on CA1 PC proximal to the soma dendrites improve the recall performance of the microcircuit model at different levels of pattern loading. The model showed that BSC acts as a threshold mechanism to remove spurious activity as larger number of patterns were stored and its synaptic thresholding efficiency was *best* dynamically controlled by PC feedback excitation to BSC near-the-soma dendrites (SO dendrites) (model 5) and

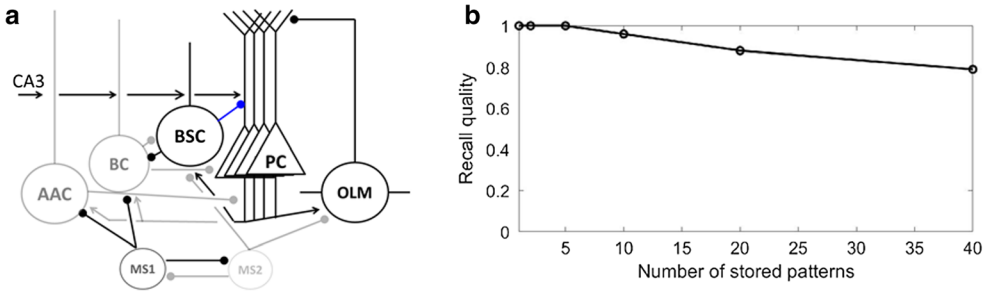

Fig. 7 **a** CA1 circuit model 2. Increased BSC feedforward inhibition to PC dendrites (depicted as blue solid line) as the number of stored patterns is increased. **b** Recall quality of the model as a function of number of patterns stored. Recall quality is perfect ($C = 1$) for the first 20 patterns stored. When 40 patterns are loaded, the mean recall quality drops to 0.79. Note that the possible minimum quality when all cells become active is 0.44

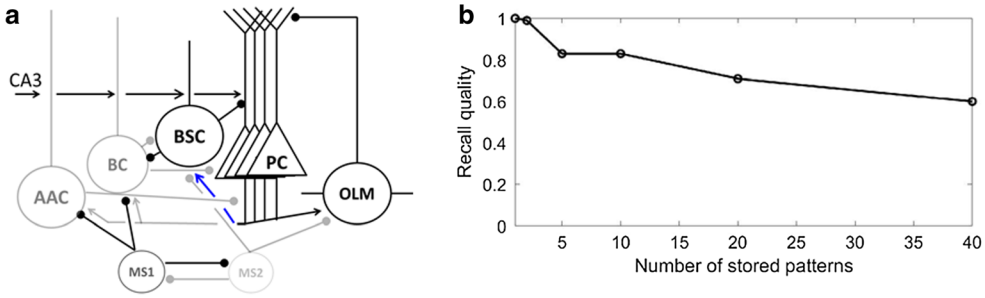

Fig. 8 **a** CA1 circuit model 3. Increased PC feedback excitation to BSC SO dendrites (depicted as blue solid line) as the number of stored patterns is increased. **b** Recall quality of the model as a function of number of patterns stored. Mean recall quality decreased even for the first five stored patterns ($C = 0.83$). For 40 stored patterns, the mean recall quality was 0.6. Note that the possible minimum quality when all cells become active is 0.44

not by CA3 feedforward excitation to BSC SR dendrites (model 4). Although the performances of models 4 and 5 were comparable for the first 20 stored patterns, when the number of stored patterns doubled, the recall quality of model 4 ($C = 0.64$) was greatly decreased compared to model 5 ($C = 0.8$). This is due to greater attenuation of dendritic spikes at BSC SR dendrites relative to the attenuation of dendritic spikes at BSC SO dendrites, resulting BSC firing rate to be smaller in the former case (when CA3 Schaffer collateral input excited the BSC) than in the latter one (when PC feedback excitation excited the BSC). The model further predicted that the BSC inhibitory threshold must be dynamic (not static as in Cutsuridis et al. [10] study), and it must monotonically increase as a function of increased stored memory patterns. This makes sense because increases in pattern loading in PC SR synapses results in more pattern PCs to fire, which in turn increase the feedback excitation to BSC, and thus its firing rate and synaptic efficacy.

Comparison with Other Models

Over the years, many theoretical attempts have been made to identify the mechanisms of memory formation, encoding and retrieval and how they are influenced as more and more memories are loaded into the system [2, 5, 16, 21, 22, 24, 36, 37, 39]. These attempts, however, lacked any biological realism.

Few notable brain mimetic attempts of testing the recall performance under varying memory loads and external stimulations have been made [18, 32, 33]. Sommer and Wennekers [32, 33] extended the original hippocampal content-addressable memory model [22, 24, 37] to investigate its memory capacity and robustness of efficient retrieval under varying memory loads and types of external stimulation (tonic and pulsed). The role of inhibition confined to basket cells acting to threshold PC activity during pattern recall was examined. A clipped synaptic modification rule of the Willshaw model was used to "induce" learning (storage) in their model [37]. Memory patterns were sequences of binary numbers (1 or 0), and each pattern was presented to a fixed number of cells in the network and each cell was active in more than one memory pattern. The participating neurons had rhythmic activity in the gamma-frequency range (30–80 Hz). If the input was switched from one memory to another, the network activity followed this change within one or two gamma cycles. With pulsed stimulation, memories were no longer attractors and they were retrieved within one or two

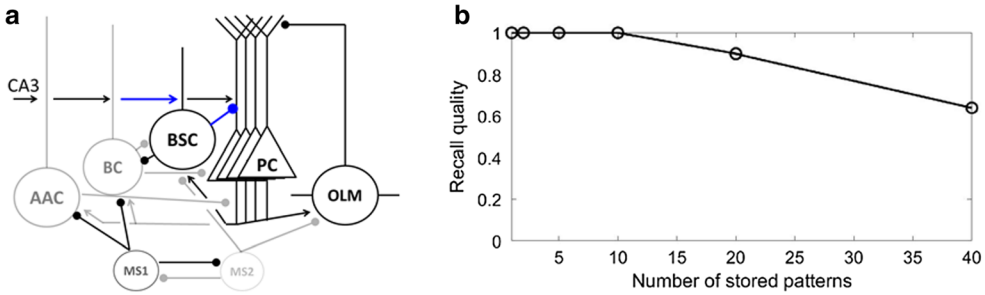

Fig. 9 **a** CA1 circuit model 4. Increased CA3 feedforward excitation to BSC SR dendrites (depicted as blue solid line) and increased BSC feedforward inhibition to PC dendrites (depicted as blue solid line) as the number of stored patterns is increased. **b** Recall quality of the model as a function of number of patterns stored. Mean recall quality is perfect ($C = 1$) for the first 10 patterns stored, drops slightly ($C = 0.9$) for 20 stored patterns and settles to 0.64 for 40 stored patterns. Note that the possible minimum quality when all cells become active is 0.44

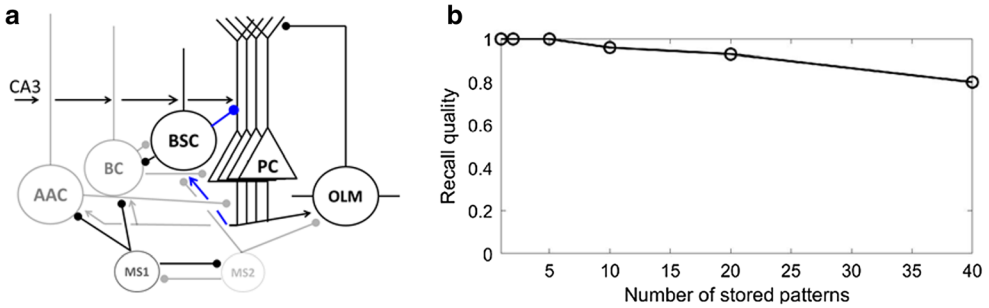

Fig. 10 **a** CA1 circuit model 5. Increased BSC feedforward inhibition to PC dendrites (depicted as blue solid line) and increased PC feedback excitation to BSC SO dendrites (depicted as blue solid line) as the number of stored patterns is increased. **b** Recall quality of the model as a function of number of patterns stored. Mean recall quality is perfect ($C = 1$) for 20 patterns but drops to 0.8 when 40 patterns are loaded. Note that the possible minimum quality when all cells become active is 0.44

gamma cycles. Burst of firing became relevant for coding and its occurrence was used for discriminating related processes from background activity.

Another notable study was the work by Hunter and colleagues [18] which compared and contrasted the performance of the Sommers and Wennekers model with previously published recall results of the Willshaw model [14, 15]. They tested how well the network can recall a pattern when there is full (100%) or partial (10%) connectivity or corruption due to noise and how the global inhibitory threshold could implement the winner-take-all (WTA) recall of a stored pattern. Biophysical implementations of three separate WTA recall methods were used: (1) standard WTA implemented by intrinsic PC thresholding (increases in Na^+ density and membrane resistance) and global inhibition; (2) normalized WTA implemented by localized inhibition proportional to the excitation a cell could receive the range of EPSPs and the dendritic sums produced; and (3) amplified WTA via a non-linear increase of EPSP summation, so that the cells that reached a certain membrane potential increased their summed EPSP amplitude via a persistent Na^+ current. Recall was tested by tonically stimulating a subset of principal neurons in the network using an injected current of varying strength. Recall performance was tested by storing 50 random patterns, each consisting of 10 active cells, in the network and then using 5 of the 10 cells of a stored pattern as a recall cue. Recall quality with 10% connectivity was as follows: (1) 61% in standard WTA, (2) 64% in normalized WTA and (3) 65% in amplified WTA.

My model presented in this paper shared several features with these previously described models but had few notable differences. As in the Sommer and Wennekers [32, 33] and Hunter et al. [18] models, inhibition worked as a global non-constant threshold. Memory patterns were sequences of "1 s" and "0 s," and each pattern was presented to fixed number of cells in the network. Stored patterns overlapped with cells been active in more than one memory pattern. In contrast to the Sommer and Wennekers [32, 33] and Hunter et al. [18] works, in my model, the global threshold mechanism was operated by dendritic inhibition (bistratified cells) and it was adaptive (changeable) as the number of stored patterns increased. My model examined how selective modulation of feedforward and feedback excitatory and inhibitory pathways targeting BSC and/or PCs may influence the BSC thresholding capacity to remove spurious activity and improve the mean recall quality of PCs as a larger number of memories are stored. Of all potential modulated pathways tested, simulations showed that an adaptive threshold level set by feedforward dendritic inhibition to PC dendrites leads to a twofold improvement to recall performance with or without increased feedback excitation.

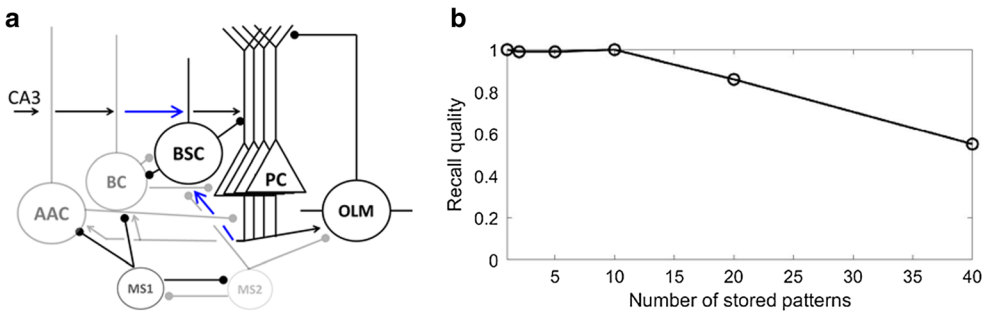

Fig. 11 **a** CA1 circuit model 6. Increased CA3 feedforward excitation to BSC SR dendrites (depicted as blue solid line) and increased PC feedback excitation to BSC SO dendrites (depicted as blue solid line) as the number of stored patterns is increased. **b** Recall quality of the model as a function of number of patterns stored. Mean recall quality for the first 10 patterns was perfect ($C = 1$), but decreased to 0.86 and 0.55 for 20 and 40 patterns, respectively. Note that the possible minimum quality when all cells become active is 0.44

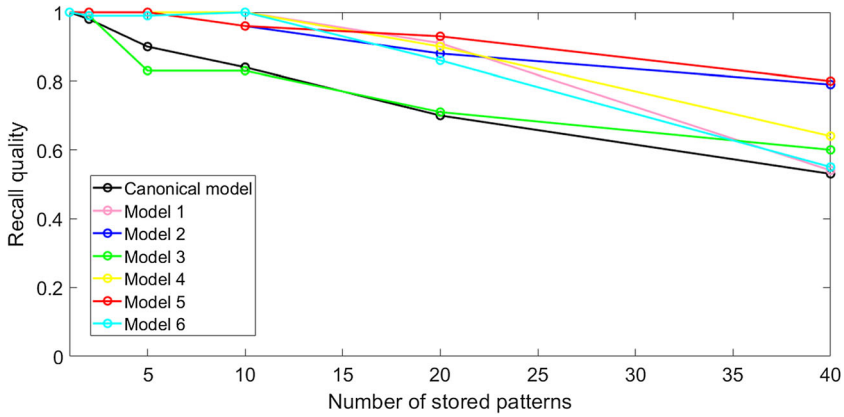

Fig. 12 Comparison of mean recall qualities of all seven models as number of stored patterns is increased

Future Extensions

Several extensions to the basic idea deserve further consideration. Although in this study the synaptic efficacy (weight) of BSC was artificially increased, perhaps a biophysical model of inhibitory/excitatory synaptic plasticity in excitatory/inhibitory synapses of PC and inhibitory interneurons dendrites may delineate what may cause the increases in the BSC synaptic efficacy. Experimental evidence has shown that inhibitory synapses on pyramidal cells as well as excitatory synapses on inhibitory interneurons are also plastic and may regulate the PC firing rate ([11, 23, 25, 31, 38]). Pelletier and Lacaille [25] showed that various forms of long-term potentiation (LTP) and depression (LTD) are reported at glutamatergic synapses of interneurons in dentate gyrus (DG), CA3 and CA1 regions of the hippocampus. The presence and type of these changes in synaptic efficacy appear to depend on the interneuron subtype, including its specific role within the hippocampal network. Saraga et al. [31] showed depolarization of the reversal potential for GABA at feedforward and feedback inhibitory synapses in PC dendrites decreased the latency to the 1st spike and decreased the inter-spike interval and increased the number of output spikes in a frequency dependent manner, improving the reliability of input–output transmission. Finally, the model of the CA1 microcircuit is still very simple. More cell types and connectivities could be included in the model [6]. Further data on type-specific cell properties and their in-vivo firing patterns can be incorporated [34].

Conclusions

In summary, the recall performance of a brain mimetic microcircuit model of the hippocampus as the number of stored patterns increased was examined when the synaptic strength of different excitatory and inhibitory pathways was selectively modulated. Out of the seven models tested, simulation results showed that an adaptive threshold level set by feedforward dendritic inhibition to PC dendrites leads to a twofold improvement to recall performance with or without increased feedback excitation. The study furthers our understanding of how memories are retrieved by a brain microcircuit. The findings provide fundamental insights into the inner workings of learning and memory in the brain, which may lead to potential strategies for treatments in memory-related disorders.

Compliance with Ethical Standards

Conflict of Interest The author declares that he has no competing interests.

Ethical Approval This article does not contain any studies with human participants or animals performed by any of the authors.

References

1. Amaral D, Lavenex P. Hippocampal neuroanatomy. In: Andersen P, Morris R, Amaral D, Bliss T, O'Keefe J, editors. The hippocampus book. Oxford: University Press; 2007. p. 37–114.
2. Amit DJ. Modeling brain function: the world of attractor neural networks. New York: Cambridge University Press; 1989.
3. Andersen P, Morris R, Amaral D, Bliss T, O'Keefe J. The hippocampus book. Oxford: University Press; 2007.
4. Borhegyi Z, Varga V, Szilagyi N, Fabo D, Freund TF. Phase segregation of medial septal GABAergic neurons during hippocampal theta activity. J Neurosci. 2004;24:8470–9.
5. Buckingham J, Willshaw D. On setting unit thresholds in an incompletely connected associative net. Network. 1993;4:441–59.
6. Chamberland S, Topolnik L. Inhibitory control of hippocampal inhibitory neurons. Front Neurosci. 2012;6:165.
7. Cutsuridis V, Hasselmo M. GABAergic modulation of gating, timing and theta phase precession of hippocampal neuronal activity during theta oscillations. Hippocampus. 2012;22:1597–621.
8. Cutsuridis V, Poirazi P. A computational study on how theta modulated inhibition can account for the long temporal delays in the entorhinal-hippocampal loop. Neurobiol Learn Mem. 2015;120:69–83.
9. Cutsuridis V, Wenneckers T. Hippocampus, microcircuits and associative memory. Neural Netw. 2009;22(8):1120–8.
10. Cutsuridis V, Cobb S, Graham BP. Encoding and retrieval in the hippocampal CA1 microcircuit model. Hippocampus. 2010;20:423–46.

11. de Luca E, Ravasenga T, Petrini EM, Polenghi A, Nieus T, Guazzi S, et al. Inter-synaptic lateral diffusion of GABAA receptors shapes inhibitory synaptic currents. Neuron. 2017;95(1):63–69.e5.
12. Freund TF, Buzsaki G. Interneurons of the hippocampus. Hippocampus. 1996;6:347–470.
13. Ganter P, Szucs P, Paulsen O, Somogyi P. Properties of horizontal axo-axonic cells in stratum oriens of the hippocampal CA1 area of rats in vitro. Hippocampus. 2004;14:232–43.
14. Graham B, Willshaw D. Improving recall from an associative memory. Biol Cybern. 1995;72:337–46.
15. Graham B, Willshaw D. Capacity and information efficiency of the associative net. Network. 1997;8:35–54.
16. Hasselmo M, Bodelon C, Wyble B. A proposed function of the hippocampal theta rhythm: separate phases of encoding and retrieval of prior learning. Neural Comput. 2002;14:793–817.
17. Hines ML, Carnevale T. The NEURON simulation environment. Neural Comput. 1997;9:1179–209.
18. Hunter R, Cobb S, Graham BP. Improving associative memory in a network of spiking neurons. In: Kurkova V, et al., editors. Lecture notes in computer science (LNCS 5164). Berlin Heidelberg: Springer-Verlag; 2008. p. 636–45.
19. Klausberger T, Magill PJ, Marton LF, David J, Roberts B, Cobden PM, et al. Brain-state- and cell-type-specific firing of hippocampal interneurons in vivo. Nature. 2003;421:844–8.
20. Klausberger T, Marton LF, Baude A, Roberts JD, Magill PJ, Somogyi P. Spike timing of dendrite-targeting bistratified cells during hippocampal network oscillations in vivo. Nat Neurosci. 2004;7:41–7.
21. Levy W. A sequence predicting CA3 is a flexible associator that learns and uses context to solve hippocampal-like tasks. Hippocampus. 1996;6:579–90.
22. Marr D. A simple theory of archicortex. Philos Trans R Soc Lond Ser B Biol Sci. 1971;262(841):23–81.
23. Mendoza E, Galarraga E, Tapia D, Laville A, Hernandez-Echeagaray E, Bargas J. Differential induction of long term synaptic plasticity in inhibitory synapses of the hippocampus. Synapse. 2006;60(7):533–42.
24. Palm G. On associative memories. Biol Cybern. 1980;36:9–31.
25. Pelletier JG, Lacaille JC. Long-term synaptic plasticity in hippocampal feedback inhibitory networks. Prog Brain Res. 2008;169:241–50.
26. Petersen CCH, Malenka RC, Nicoll RA, Hopfield JJ. All-or none potentiation at CA3-CA1 synapses. Proc Natl Acad Sci U S A. 1998;95:4732–7.
27. Poirazzi P, Brannon T, Mel BW. Arithmetic of subthreshold synaptic summation in a model CA1 pyramidal cell. Neuron. 2003a;37:977–87.
28. Poirazzi P, Brannon T, Mel BW. Pyramidal neuron as a 2-layer neural network. Neuron. 2003b;37:989–99.
29. Santhakumar V, Aradi I, Soltetz I. Role of mossy fiber sprouting and mossy cell loss in hyperexcitability: a network model of the dentate gyrus incorporating cells types and axonal topography. J Neurophysiol. 2005;93:437–53.
30. Saraga F, Wu CP, Zhang L, Skinner FK. Active dendrites and spike propagation in multicompartment models of oriens-lacunosum/moleculare hippocampal interneurons. J Physiol. 2003;552:673–89.
31. Saraga F, Balena T, Wolansky T, Dickson CT, Woodin MA. Inhibitory synaptic plasticity regulates pyramidal neuron spiking in the rodent hippocampus. Neuroscience. 2008;155(1):64–75.
32. Sommer FT, Wennekers T. Modelling studies on the computational function of fast temporal structure in cortical circuit activity. J Physiol Paris. 2000;94:473–88.
33. Sommer FT, Wennekers T. Associative memory in networks of spiking neurons. Neural Netw. 2001;14:825–34.
34. Somogyi P, Katona L, Klausberger T, Lasztóczi B, Viney TJ. Temporal redistribution of inhibition over neuronal subcellular domains underlies state-dependent rhythmic change of excitability in the hippocampus. Philos Trans R Soc Lond Ser B Biol Sci. 2013;369(1635):20120518.
35. Steinbuch K. Non-digital learning matrices as preceptors. Kybernetik. 1961;1:117–24.
36. Treves A, Rolls E. Computational constraints suggest the need for two distinct input systems to the hippocampal CA3 network. Hippocampus. 1992;2:189–200.
37. Willshaw D, Buneman O, Longuet-Higgins H. Non-holographic associative memory. Nature. 1969;222:960–2.
38. Zarnadze S, Bäuerle P, Santos-Torres J, Böhm C, Schmitz D, Geiger JR, et al. Cell-specific synaptic plasticity induced by network oscillations. Elife. 2016;5:e14912.
39. Zhang S, Huang K, Hussain A. Learning from few samples with memory network. Cogn Comput. 2018;10(1):15–22.